Published in final edited form as:
J Immunol. 2014 June 1; 192(11): 5245–5256. doi:10.4049/jimmunol.1400111.

Structural and Functional Correlates of Enhanced Anti-viral Immunity Generated by Heteroclitic CD8 T Cell Epitopes[1]

Jonathan A. Trujillo[*,a], **Stephanie Gras**[†,a], **Kelly-Anne Twist**[†], **Nathan P. Croft**[†], **Rudragouda Channappanavar**[‡], **Jamie Rossjohn**[†,#,^,b], **Anthony W. Purcell**[†,b], and **Stanley Perlman**[*,‡,b]

[*]Interdisciplinary Program in Immunology, University of Iowa, Iowa City, IA 52242

[†]Department of Biochemistry and Molecular Biology, School of Biomedical Sciences, Monash University, Clayton, Victoria 3800, Australia

[#]Institute of Infection and Immunity, Cardiff University School of Medicine, Heath Park, Cardiff CF14 4XN, UK

[^]Australian Research Council Centre of Excellence in Advanced Molecular Imaging, Monash University, Clayton, Victoria 3800, Australia

[‡]Department of Microbiology, University of Iowa, Iowa City, IA 52242

Abstract

Peptides that bind poorly to MHC class I molecules often elicit low functional avidity T cell responses. Peptide modification by altering the anchor residue facilitates increased binding affinity and may elicit T cells with increased functional avidity towards the native epitope (“heteroclitic”). This augmented MHC binding is likely to increase the half-life and surface density of the heteroclitic complex but precisely how this enhanced T cell response occurs *in vivo* is not known. Furthermore, the ideal heteroclitic epitope will elicit T cell responses that completely cross-react with the native epitope, maximizing protection and minimizing undesirable off-target effects. Such epitopes have been difficult to identify. Here, using mice infected with a murine coronavirus that encodes epitopes that elicit high (S510, CSLWNGPHL) and low (S598, RCQIFANI) functional avidity responses, we show that increased expression of peptide S598 but not S510 generated T cells with enhanced functional avidity. Thus immune responses can be augmented towards T cell epitopes with low functional avidity by increasing antigen density. We also identified a heteroclitic epitope (RC**V**IFANI) that elicited a T cell response with nearly complete cross-reactivity with native epitope and demonstrated increased MHC-peptide abundance compared to native S598. Structural and thermal melt analyses indicated that the Q600V substitution enhanced stability of the peptide-MHC complex without greatly altering the antigenic surface, resulting in highly cross-reactive T cell responses. Our data highlight that increased pMHC complex display

[1]This research was supported by a NIH grant (R01 NS036592) and a National Health and Medical Research Council of Australia (NHMRC) Project grant (1023141). A.W.P. is a NHMRC Senior Research Fellow. J.R. is an NHMRC Australia Fellow. J.A.T. was supported by a predoctoral individual NRSA NIH grant (AI093129). S.G. is an ARC Future Fellow.

Corresponding author for submission: Stanley Perlman, M.D., Ph.D.. Tele # 319-335-8549; FAX: 319-335-9006; stanley-perlman@uiowa.edu.
[a]JAT and SG contributed equally to this work.
[b]Joint senior and corresponding authors.

contributes to heteroclitic epitope efficacy and describe parameters for maximizing immune responses that cross-react with the native epitope.

INTRODUCTION

Pathogen and tumor clearance both require effective T cell responses; therefore, any vaccines designed to enhance immune protection against infectious diseases or cancer should include relevant CD8 or CD4 T cell epitopes (1, 2). However, some subdominant epitopes recognized in infectious settings and from many tumors induce weak, low functional avidity T cell responses that are neither protective against pathogen exposure nor efficacious in diminishing tumor burden (3–9). Several approaches have been used to enhance the functional avidity of T cell responses to tumor and viral antigens, including use of potent adjuvants during immunization (10), adoptive immunotherapy of high-avidity T cell clones (11, 12), and immunization with optimized peptides, including heteroclitic peptides; the latter, although altered in sequence, result in augmented T cell responses to the native epitope (2, 13, 14).

Heteroclitic CD8 T cell epitopes were initially identified in the context of tumors (13). In most instances, heteroclitic peptides display enhanced binding to the MHC molecule (15, 16), although heteroclitic peptides that augment binding to the TCR have also been identified (e.g. (17)). Heteroclitic epitopes exhibiting augmented MHC class I (MHCI) binding and potentially, greater effective peptide MHC complex (pMHC)[2] surface density, may induce a higher functional avidity T cell response. However, whether increased pMHCI levels actually result in enhanced functional avidity has not been established because several *in vitro* studies showed that low levels of peptide expressed on the surface of APCs induced CD8 T cells with high functional avidity. Conversely, higher levels of pMHCI expression resulted in the outgrowth of cells with lower avidity for the pMHCI (3). Based on these *in vitro* observations, weakly immunogenic epitopes, which often result from low affinity pMHCI interactions and subsequently exhibit low pMHCI density, would be predicted to induce high functional avidity responses. The relationship between the level of pMHCI on the surface of APCs and the subsequent CD8 T cell response has also been investigated *in vivo* (18–20). Increased epitope density raised the magnitude of the response but did not affect the functional avidity of the primary immune response. Importantly, none of these *in vitro* or *in vivo* studies have examined the relationship between pMHCI density and functional avidity of the T cell response elicited towards a weakly immunogenic epitope and its corresponding heteroclitic analogue.

One concern with the use of heteroclitic epitopes is that a variable fraction of the response may recognize only the modified and not the native epitope (21). The outgrowth of cells that recognize only the modified epitope is not only futile as a vaccine strategy but raises the possibility that the modified epitope-specific response could also respond to a self-epitope.

[2]Abbreviations. pMHC-peptide MHC complex; JHMV-JHM strain of mouse hepatitis virus; rJ-recombinant version of JHMV; SARS-CoV-Severe Acute Respiratory Syndrome coronavirus; VacV-vaccinia virus; p.i.-post infection; TFA-trifluoroacetic acid; CD-circular dichroism; LC-MRM-MS-Liquid chromatography-multiple reaction monitoring-mass spectrometry; IDA- information-dependent acquisition; PEG- polyethylene glycol; aba-aminobutyric acid; r.m.s.d.-root mean square deviation.

This could initiate or contribute to the development of autoimmune disease, thus making the use of heteroclitic peptides in clinical settings problematic.

Mice infected with a murine coronavirus, the neurotropic JHM strain of mouse hepatitis virus (JHMV or its recombinant form, rJ), develop acute encephalitis and acute and chronic demyelinating diseases (22). Of note, JHMV is a member of the same group of coronaviruses as two pathogenic human coronaviruses associated with severe respiratory disease (Severe Acute Respiratory Syndrome-coronavirus (SARS-CoV) and Middle East Respiratory Syndrome-CoV) (23). The CD8 T cell response to JHMV in C57BL/6 mice is directed at two epitopes, spanning residues 510–518 and 598–605 of the surface glycoprotein (CSLWNGPHL, S510, H-2D^b-restricted and RCQIFANI, S598, H-2K^b-restricted) (24). Epitope S510 is immunodominant, induces a high functional avidity response, and in some settings, undergoes mutation as part of viral evasion of the T cell response (25). Epitope S598 is subdominant and binds with lower affinity to the MHC class I molecule than peptide S510 (14). Further, the low functional avidity response to epitope S598 is unable to protect mice after infection with virus mutated in S510 (26). With the goal of enhancing the S598-specific response, we optimized peptide binding to K^b by changing a secondary anchor residue at position three of the epitope from Gln to Tyr to match the consensus motif for K^b binding (RC**Y**IFANI; Q600Y) (14). We showed that the modified peptide enhanced the stability of pMHCI and induced CD8 T cells with higher functional avidity towards the native form of the S598 epitope. However, as in other studies of heteroclitic epitopes, we found that a substantial fraction (~35%) of the responding T cells recognized only the variant Q600Y epitope. For the reasons described above, this level of cross-reactivity would be unsuitable in a clinical setting because part of the T cell response would be ineffectual (i.e., these T cells would recognize only the heteroclitic peptide and would not contribute to a protective immune response) and could potentially recognize a self-epitope.

Here, we investigated a putative mechanism of action of heteroclitic epitopes, designed around the subdominant JHMV S598 epitope. If heteroclitic epitopes function by increasing the effective epitope density on the surface of APCs, one would predict that increasing surface density of the native epitope by another mechanism would also result in the induction of a high functional avidity T cell response. To evaluate this possibility, we used a vaccinia virus (VacV)-based experimental system to vary K^b/S598 abundance on APCs. The results showed that increased pMHCI expression of epitope S598, which induces a low functional avidity response, but not of epitope S510, which stimulates a high functional avidity response in rJ-infected mice, resulted in the selection of CD8 T cells with enhanced ability to respond to the epitope. We also addressed the problem of selection of T cells that responded to variant but not native epitope by using the crystal structures of K^b/S598 and K^b/Q600Y (14) to identify additional mutations at subanchor position 3 that were predicted to be heteroclitic. We showed that one heteroclitic S598 analogue (Q600V) elicited a T cell response that nearly completely cross-reacted with the native epitope. Consistent with the notion that surface density is a major factor in how heteroclitic epitopes function, levels of both K^b/Q600V and K^b/Q600Y were increased compared to K^b/S598.

MATERIALS AND METHODS

Mice

Six to eight week old pathogen-free C57BL/6 (B6) mice were purchased from the National Cancer Institute (Frederick, MD, USA) and housed in the Animal Care Facility at the University of Iowa. This study was carried out in strict accordance with the recommendations in the Guide for the Care and Use of Laboratory Animals of the National Institutes of Health. Animal experiments were approved by the Institutional Animal Care and Use Committee at the University of Iowa.

Viruses

Recombinant JHMV (rJ) was propagated on 17Cl-1 cells and titered on HeLa cells expressing the MHV receptor, CEACAM1 (27) as previously described (28). VacV-S510, -S598, -$S598_{Q600Y}$ and -$S598_{Q600V}$ were engineered using complementary oligonucleotides containing the DNA sequence of the identified epitope, an amino-terminal methionine and appropriate restriction enzyme sequences. Oligonucleotides for the S510 construct were previously published (24). Oligonucleotides used for the S598 constructs were: forward: TCGACGCCACCATGAGGTGC(**CAA,TAC,GTG**)ATCTTCGCCAACATCTAAGGTAC and reverse: CTTAGATGTTGGCGAAGAT(**TTG**,**GTA,CAC,**)GCACCTCATGGTGGCG, where the bolded nucleotides encode amino acids Gln, Tyr, Val, respectively. The oligonucleotides were annealed and ligated into PSC65 (a VacV shuttle vector with a strong synthetic VacV early/late promoter for expressing the gene of interest, kindly provided by Dr. B. Moss, National Institutes of Health). VacV-S was constructed by inserting a deleted S gene (lacking the transmembrane domain (24)) into pSC65. Mice were infected intraperitoneally with 2×10^7 PFU of recombinant VacV and $CD8^+$ T cell responses measured in the spleen. Recombinant JHMV expressing variant S598 epitopes were engineered as previously described (14). Mutations were introduced using a site directed mutagenesis kit (QuikChange II Site-Directed Mutagenesis Kit (Stratagene, La Jolla CA)) and the following primers: Q600V fwd: CACTTGTTTAGTAAATGATCGCTGCGTGATTTTTGCTAACATATTGTTAAATGG; Q600V rev: CCATTTAACAATATGTTAGCAAAAATCACGCAGCGATCATTTACTAAACAAGTG; Q600F fwd: CACTTGTTTAGTAAATGATCGCTGCTTCATTTTTGCTAACATATTGTTAAATGG; Q600F rev: CCATTTAACAATATGTTAGCAAAAATGAAGCAGCGATCATTTACTAAACAAGTG. Underlined nucleotides correspond to the Gln to Val or Phe changes. At least two independent isolates of each recombinant virus were propagated and analyzed.

One step viral growth kinetics

Virus was inoculated onto confluent 17Cl-1 cells at a multiplicity of infection of 0.1. Cells were harvested at the indicated time points and total virus (cell-associated and cell-free) was titered as previously described (14).

Purification of MHC-peptide complexes

DC2.4 cells (1×10^8), grown as previously described (29), were infected with VacV-S598, VacV-$S598_{Q600Y}$, VacV-$S598_{Q600V}$, VacV-S510 or VacV-S at 5 PFU/cell and incubated for 4 hours before snap freezing. DC2.4 cells were disrupted by gentle resuspension in a total of 5 ml of lysis buffer (0.5% IGEPAL (Sigma), 50 mM Tris pH 8, 150 mM NaCl and protease inhibitors (Complete Protease Inhibitor Cocktail Tablet; Roche Molecular Biochemicals)). DC2.4s were disrupted by gentle resuspension in a total of 5 ml of lysis buffer without cryogenic milling. Lysates were incubated with rotation for 1 h at 4 °C and cleared by centrifugation. MHC-peptide complexes were immunoaffinity purified using specific monoclonal antibodies 28-14-8S (anti-H-$2D^b$) or Y-3 (anti-H-K^b) bound to protein A-Sepharose, as previously described (29). Bound complexes were eluted by acidification with 10% acetic acid. The mixture of peptides and MHC protein chains was fractionated on a 4.6 mm internal diameter × 50 mm long reversed-phase C18 HPLC column (Chromolith Speed Rod, Merck) using an ÄKTAmicro™ HPLC system (GE Healthcare) running on a mobile phase buffer A of 0.1% trifluoroacetic acid (TFA) and buffer B of 80% acetonitrile/ 0.1% TFA and at a flow rate of 1 ml/min with peptides separated across a gradient of 2% B to 45% B over the course of 20 minutes, collecting 500 µl fractions.

Liquid chromatography-multiple reaction monitoring-mass spectrometry (LC-MRM-MS)

Following peptide elution, samples were concentrated, treated with TCEP (5 mM) for 30 minutes at 60°C and immediately analysed by mass spectrometry. An AB SCIEX QTRAP® 5500 mass spectrometer was used for MRM detection, coupled on-line to a Eksigent nano LC and Nanoflex cHiPLC manifold (Eksigent). 10 µl samples were injected and loaded onto a trap column (200 µm × 0.5 mm ChromXP C18-CL 3 µm 120 Å) at a flow rate of 10 µl/min in 98% water, 2% acetonitrile and 0.1% formic acid for 10 minutes. For on-line fractionation of samples onto the mass spectrometer, samples were eluted from the trap column and passed over a cHiPLC analytical column (75 µm × 15 cm ChromXP C18-CL 3 µm 120 Å) at 300 nl/min under the following buffer B (98% acetonitrile, 0.1 % formic acid in water) gradient conditions: 0–3 min 2–10% B, 3–33 min 10–40% B, 33–36 min 40–80% B, 36–38 min hold at 80% B, 38–39 min 80–2% B, followed by equilibration at 2% B until the end of the run at 48 min. The QTRAP® 5500 was operated in MRM mode in unit resolution for Q1 and Q3, coupled to an information-dependent acquisition (IDA) criterion set to trigger an EPI scan (10,000 Da/sec; rolling CE; unit resolution) following any MRM transition exceeding 500 counts. Optimal MRM Q1>Q3 transition conditions were designed through analysis of synthetic peptides and are listed in Table 1. Data analysis was performed using Analyst v1.5.2 (AB SCIEX). Isotopically labelled S598 (S598*, containing a modified isoleucine: (^{13}C)6, (^{15}N)1, mass shift of +7 Da, Mimotopes, Clayton, AU) was added to samples prior to analysis to control for losses during processing and to provide absolute quantitation as previously described (30).

Circular Dichroism

Circular dichroism (CD) spectra were recorded using an AVIV 410-SF CD spectrometer. Wavelength scans were performed between 190 and 250 nm using a 1 mm path length quartz cuvette at 20°C with a sample concentration of 0.178 mg/ml in 10 mM Tris, 150 mM

NaCl, pH 8. For thermal denaturation scans, ellipticity at 218 nm was monitored between 20 and 90°C in 0.5°C steps. Data were normalized and then fit to a Boltzmann sigmoidal curve. The temperature at which 50% of the protein complex was unfolded was determined (T_m).

Preparation of brain-derived leukocytes

Brain-derived mononuclear cells were isolated as previously described (31). Briefly, mice were perfused with PBS and brains were harvested, dispersed using 25-gauge needles and digested with collagenase D (1mg/ml; Roche Diagnostics) and DNase I (0.1 mg/ml; Roche Diagnostics) at 37°C for 30 min. Mononuclear cells were isolated by passing homogenized tissue through a 70 μm cell strainer, followed by centrifugation through a 30% Percoll gradient (Pharmacia, Uppsala, Sweden).

Intracellular cytokine staining and functional avidity analysis

Mononuclear cells were harvested from the brains or spleens of mice at 7 days p.i. and analyzed for expression of IFN-γ by an intracellular cytokine assay as previously described (32). Briefly, brain-derived cells were stimulated in the presence of antigen presenting cells (CHB3 cells, B cell line, I-A^b, H-2D^b, H-2K^b) pulsed with the indicated peptide for 6 h at 37° C in the presence of 1 μl/ml Golgiplug (BD Pharmingen). Splenocytes were similarly exposed to peptides, but in the absence of exogenous antigen presenting cells. Peptides were used at a final concentration of 1 μM, unless indicated. Cells were stained with antibodies specific for CD8 (53-6.7; BD Pharmingen), CD4 (RM 4–5; BD Pharmingen) CD16/CD32 (2.4G2; BD Pharmingen), and IFN-γ (XMG1.2; eBioscience) and analyzed by flow cytometry using a FACSCalibur or a FACSVerse (BD Biosciences, Mountain View, CA). Data sets were analyzed using FlowJo software (Tree Star, Inc., Ashland, OR). To assess functional avidity, splenocytes or brain-derived mononuclear cells isolated at day 7 p.i. were stimulated with graded doses of the relevant peptide and examined for INF-γ production. The frequency of CD8 T cells producing IFN-γ at each concentration of peptide was measured and expressed as a percentage of the maximum response detected. Data were fit to sigmoidal-dose response curves and used to calculate the amount of peptide needed to reach a half maximum response (EC_{50}).

Immunization with peptide-coated DCs

Splenic DC were isolated after subcutaneous injection of B6 mice with 5×10^6 B16 cells expressing Flt3L (provided by M. Prlic and M. Bevan, University of Washington), pulsed with the indicated peptides (10 nM, 100 nM or 1 μM final concentration) and injected intravenously into mice as previously described (33). Mice were sacrificed six days later and epitope S598-specific T cell responses measured in the spleen as described above.

Protein expression, purification, crystallisation and structure determination

K^b and β2-microglobulin molecules were expressed in Escherichia coli as inclusion bodies, refolded with the Q600V or Q600F peptides and purified as previously described (34). The two pMHCI complexes were concentrated to 5 mg/ml, using the hanging-drop vapor diffusion technique at 20°C. Crystals were grown with a reservoir containing 16–24% polyethylene glycol (PEG) 3350, 0.1 M Na-Cacodylate, pH 6.5, and 0.2 M Na acetate. The

crystals belong to space group $\mathbf{P}2_1$ and the unit cell dimensions were consistent with two molecules per asymmetric units (Table 2).

The crystals were flash frozen to a temperature of 100°K before data were collected using the Australian Synchrotron (MX2 beamline with an ADSC Q305 detector). The data were processed and scaled with the XDS (35). The crystal structures were solved using the molecular replacement method in the program Phaser (36) from the CCP4 suite of programs (37). The search probe used to solve the structure was the structure of mouse MHC class I K^b minus the peptide (Protein Data Bank accession number 2ZSV) (14). The progress of refinement was monitored by the Rfree value with neither a sigma nor a low-resolution cut-off being applied to the data. This protocol includes several cycles of refinement with the PHENIX software (38) Buster (39), followed by manual model rebuilding with Coot program (40). Final refinement statistics are summarized in Table 2. The final models were validated using the Protein Data Bank validation Web site, and submitted to Protein Data Bank database (http://www.rcsb.org/pdb/home/home.do; accession numbers 4PV8 (K^b/Q600F), 4PV9 (K^b/Q600V)). The total number of intermolecular bonds was calculated using the CCP4 program suite (37) with a cut-off of 4 Å was used for the van der Waals, 3.5 Å for hydrogen-bonds and 5 Å for salt-bridges.

Statistics

Two-tailed, unpaired Student *t* tests were used to analyze differences in mean values between groups except where indicated. All results are expressed as means ± SE of the means. P values < 0.05 were considered significant.

RESULTS

Increased K^b/S598 abundance enhances functional avidity

Heteroclitic CD8 T cell epitopes often augment the stability of the pMHC, which should increase the effective surface expression of the epitope. However, whether increased surface epitope expression actually results in enhanced functional avidity is not established. Since it is not possible to increase epitope expression in the context of an rJ infection, we investigated the relationship between total pMHCI displayed and functional avidity of the T cell response, using a set of VacV that expressed epitope S598 or S510 at widely varying levels. In one construct, the epitopes were expressed from a soluble form of the S protein (VacV-S), whereas in another set of VacV constructs, epitopes S598 and S510 were expressed as minigenes (VacV-S598 and VacV-S510; Figure 1A). Previous reports indicated that epitope expression from a minigene results in elevated pMHCI surface levels and high magnitude T cell responses (41, 42). We confirmed these results using DC2.4 cells (H-2^b-restricted) infected *in vitro* with each construct, with levels of peptide S510 or S598 measured by targeted liquid chromatography-multiple reaction monitoring-mass spectrometry (LC-MRM-MS) at 4 hours post infection (p.i.) as previously described (29, 30). Examination of peptides eluted from immunoaffinity purified K^b-and D^b-peptide complexes derived from cells infected with VacV-S598 or VacV-S510 revealed detectable levels of S598 and S510 (Figure 1B). Quantification performed using an isotopically labeled S598 standard (see Materials and Methods) indicated that approximately 3000 copies of K^b/

S598 were present per infected cell (Figure 1C). In contrast, neither peptide was detectable from cells infected with VacV-S, suggesting very low levels of antigen presentation from this VacV recombinant (a limit of detection of 30–60 copies of K^b/S598 was calculated based on the efficiency of detection of the isotopically labeled S598* peptide standard) (Figure 1B–C). As a control (29), we found equivalently high levels of a VacV-derived peptide (the immunodominant K^b-restricted epitope $B8_{20\text{-}27}$, TSYKFESV) from cells infected with all three viruses (Figure 1B). Of note, we could not examine surface levels of epitopes S598 or S510 in rJ-infected cells because we could not identify a D^{b+}/K^{b+} cell line that was susceptible to efficient infection with rJ.

Next, we assessed the magnitude and functional avidity of the S598-specific CD8 T cell response induced by low (VacV-S) and high (VacV-S598) levels of S598. For this purpose, we intraperitoneally infected B6 mice with either VacV-S or VacV-S598 and assessed the magnitude of the response in the spleen at day seven p.i. by measuring the percentage of CD8 T cells producing IFN-γ in response to *ex vivo* stimulation with S598 peptide. S598-specific CD8 T cells were detected using cytokine expression because K^b/S598 tetramer exhibits poor binding and detects only a minority of S598-specific CD8 T cells identified after peptide stimulation (unpublished observations). VacV-S598 elicited a significantly higher percentage of S598-specific CD8 T cells than did VacV-S (Figure 2A).

To assess the functional avidity of the resultant S598-specific T cell populations, splenocytes from mice infected with VacV-S or VacV-S598 were stimulated with graded doses of S598 peptide and examined for IFN-γ production (Figure 2A–C). We assessed relative functional avidity by determining the peptide concentration needed to reach a half maximum response (EC_{50}). Infection with VacV-S induced a low functional avidity S598-specific CD8 T cell response, similar to that induced by S598 in the rJ-infected brain (14) or rJ in the spleen after intraperitoneal inoculation (Figure 2D). Remarkably, however, infection with VacV-S598 gave rise to a population of T cells with significantly greater sensitivity to S598, requiring approximately 1000-fold less peptide to achieve a half maximum response (Figure 2B and C). Thus, increased abundance of the K^b/S598 complex resulted in the greater accumulation of CD8 T cells with high functional avidity. An alternative explanation for these results is that peptide processing was different when S598 was expressed from a minigene versus intact S protein. However, minimal CD8 T cell responses to peptides with N or C terminal extensions or partial overlap with S598 (RCQIFANIL, RCQIFANILL, DRCQIFANI, CQIFANIL, QIFANILL) were detectable after immunization with VacV-S (data not shown) and none of these extended forms could be detected by LC-MS/MS (data not shown), together suggesting that the same formulation of epitope S598 was recognized after immunization with either VacV construct.

During JHMV infection, the immunodominant epitope S510 generates a high functional avidity CD8 T cell response (24, 43). To determine whether increasing the levels of D^b/S510 would also enhance the functional avidity of this already potent response, mice were infected with VacV-S or VacV-S510. We observed similar frequencies of CD8 T cells specific for S510 in mice infected with either virus (Figure 2E). In sharp contrast to S598, equivalently high functional avidity S510-specific CD8 T cell responses were generated in

response to infection with either VacV-S (low D^b/S510 expression) or VacV-510 (high D^b/S510 expression) (Figure 2F and G).

To address whether the functional avidity of the virus-specific response was broadly altered by infection with VacV expressing the S protein vs. a minigene construct, we examined the CD8 T cell response to VacV epitope $B8_{20\text{-}27}$. The percentages of CD8 T cells specific for $B8_{20\text{-}27}$ were similar in the spleens of mice infected with VacV-S, VacV-S598 or VacV-S510 (Figure 2H). Additionally, each virus construct induced high functional avidity $B8_{20\text{-}27}$-specific CD8 T cell responses, with equivalent EC_{50} values (Figure 2I and J). Taken together, these results suggest that the observed differences in the functional avidity of the T cell responses to S598 are most likely the consequence of different levels of cognate antigen.

Heteroclitic S598 analogues induce higher functional avidity S598-specific CD8 T responses

We previously showed that, while the heteroclitic Q600Y peptide elicited a higher functional avidity S598-specific CD8 T cell response than the native S598 epitope, only a fraction of Q600Y-primed cells recognized the native epitope (14). An ideal heteroclitic analogue would increase the number of high affinity virus-specific effectors, while minimizing the expansion of cells that fail to recognize the native viral epitope. To try to achieve this, we selected four additional amino acid substitutions (Val, Phe, Glu, Pro) at position three of the S598 epitope that were predicted to be heteroclitic based on our previous work (14). These modifications were chosen because they are non-homologous, bulky substitutions, similar to the Gln to Tyr change in our original study. Gln has a polar uncharged side chain, Val, Phe and Pro, like Tyr, contain hydrophobic side chains and Glu is a charged homolog of Gln. One of these variants (Q600E, RC**E**IFANI) was not immunogenic when examined in preliminary experiments (data not shown). We engineered recombinant JHMV encoding the Q600F or Q600V substitutions ($rJ.S598_{Q600F}$ and $rJ.S598_{Q600V}$) (Figure 3A), but could not develop a recombinant virus containing the Q600P substitution, most likely because the P substitution was detrimental to virus viability. As shown in Figure 3B, both $rJ.S598_{Q600F}$ and $rJ.S598_{Q600V}$ exhibited similar *in vitro* growth kinetics as JHMV encoding native S598 (rJ), indicating that the mutations do not greatly affect virus fitness. Initially, we showed that, like Q600Y (14), Q600F and Q600V enhanced the thermostability of the K^b/peptide complexes (Tm= 62.7±0.4°C and Tm=60.2±0.2°C, respectively) compared to wild type K^b/S598 (Tm=56.2±1.9°C) (Figure 3C). Efficient K^b/S598 complex formation required substitution of the cysteine of the peptide (R**C**QIFANI) with L-α-aminobutyric acid (Aba, an isostereomer of cysteine). This modification at the P2-Cys does not affect epitope recognition (14). Thus Aba-modified peptides were used in both these analyses and the structural studies below.

We next examined the epitope-specific CD8 T cell responses in the brains of B6 mice intranasally infected with rJ or one of its variants. In mice infected with $rJ.S598_{Q600Y}$ (Figure 4A and B), $rJ.S598_{Q600F}$ (Figure 4C and D) or $rJ.S598_{Q600V}$ (Figure 4E and F), a high frequency (35–40%) of brain-derived CD8 T cells recognized their cognate antigen with the variant S598-specific T cell response emerging as the immunodominant population. Concomitantly, the frequency of the S510-specific T cell response contracted relative to that

induced in mice infected with wild type rJ (summary data shown in Figures 4B, D and F). Additionally, the majority of the CD8 T cells primed by each of the variants cross-reacted to native S598 (summarized in Figure 4G). Approximately 75% of CD8 T cells primed by Q600Y or Q600F produced IFN-γ when stimulated with native S598 peptide (Figures 4A–D and summarized in Figure 4G). Most notably, Q600V induced the greatest proportion of cells with the desired specificity, with nearly all (~98%) of the Q600V-reactive T cells also recognizing native S598 (Figures 4E and F and summarized in Figure 4G). In addition, cells primed by Q600F or S598 exhibited the greatest level of bidirectional cross-reactivity, with the majority of the S598-primed cells recognizing the Q600F variant (Figure 4C and summarized in Figure 4D). In contrast, only a small fraction of S598-primed CD8 T cells recognized Q600Y or Q600V peptide (Figures 4A and E, upper right panels and summarized in Figures 4B and F).

Since all of the S598 variants primed high magnitude responses to S598, we next determined whether these responses exhibited higher functional avidity when reacted against S598 peptide than those induced by the native epitope. As shown in Figure 5, all of the variants gave rise to CD8 T cell responses with lower EC_{50} than observed in rJ-infected mice. Cells primed by $rJ.S598_{Q600Y}$ or $rJ.S598_{Q600F}$ required approximately 10-fold less peptide (EC_{50}: 1.7×10^{-8} M; EC_{50}: 1.3×10^{-8} M, respectively) than did the rJ-primed cells (EC_{50}: 1.5×10^{-7} M) to achieve a half-maximum response, while CD8 T cells selected by $rJ.S598_{Q600V}$ (EC_{50}: 2.2×10^{-9} M) exhibited even greater potency for S598 (Figures 5A and B). These results indicate that peptide Q600V is an ideal heteroclitic epitope, inducing a high avidity, highly cross-reactive response to the native S598 epitope.

The results described in Figure 2 suggest that higher K^b/S598 complex density resulted in a T cell response with higher functional avidity. To determine whether K^b/Q600V or K^b/Q600Y was also displayed at a higher density, we used two complementary approaches. First, we infected DC2.4 cells with VacV expressing S598, Q600V or Q600Y as minigenes and assayed the expression of MHCI complexed with each peptide. Levels of peptide were lower from cells infected with VacV-S598 compared to cells infected with VacV expressing either variant (Figure 6A), while levels of VacV-specific epitopes ($B8_{20\text{-}27}$) were similar in all infections. In a second approach, we reasoned that since S598 bound less stably to MHCI than the variant peptides, it would exhibit lower surface levels after pulsing and washing. If this occurred, DCs coated with S598 would be expected to induce a lower CD8 T cell response after inoculation into mice and this response should be of lower functional avidity. To address this possibility, we immunized mice with DCs pulsed with S598 or Q600V peptide and measured T cell responses. As shown in Figure 6B, responses were detected to both peptides, but were much lower to S598 than Q600V; the response to S598 was so low that it precluded further analyses of functional avidity. Together, these results suggest that the surface levels of the epitopes with higher functional avidity (Q600Y and Q600V) were substantially higher than levels of S598 when expressed endogenously or after loading exogenously and a period of chase *in vivo*.

Structures of H-2K^b in complex with the heteroclitic Q600V and Q600F peptides

To understand the structural requirements for the generation of heteroclitic peptides that elicit almost exclusively cross-reactive T cells, such as the Q600V analogue, we determined the crystal structures of K^b/Q600V and K^b/Q600F, and compared these to those of K^b/S598 and K^b/Q600Y (Figure 7), which we previously determined (14). As in the thermostability experiments (Figure 3C), the use of Aba-modified peptides was required for efficient K^b/S598 complex formation. The structures of the K^b molecule in complex with the Q600V and Q600F mutants of the S598 epitope were solved to a resolution of 2.0 and 2.3 Å respectively (Table 1). The structures of the pMHCI were consistent with the previously solved K^b structure in complex with the wild-type S598 epitope (Figure 7A), with a root mean square deviation (r.m.s.d.) of 0.25 Å of the Cαs on the α1α2 domains of the K^b molecule (Figure 7). The peptides adopted a similar conformation to that observed for the S598 epitope, namely P1-Arg, P4-Ile and P7-Asn were solvent exposed whereas P2-Aba, P3-Val/Phe, P5-Phe and P8-Ile were buried in the antigen-binding cleft (Figure 7). The peptides shared a highly similar structure, with a r.m.s.d. of 0.10 and 0.14 Å on the Cα atoms, respectively for the Q600V (Figure 7D) and Q600F (Figure 7C) compared to the native S598 epitope. Thus, there were minimal structural perturbations in the pMHCI structures relative to the wild type complex (Figure 7E, F).

The three heteroclitic pMHC complexes exhibit a higher T_m than the native S598 pMHC complex ((Figure 3C) and (14)), which was associated with a higher number of intermolecular bonds observed in the pMHC structures, calculated using the CCP4 program suite as described in the Materials and Methods (169, 175, 190, 194 intermolecular bonds for S598, Q600V, Q600Y and Q600F respectively, Table 3). Next we addressed whether the higher number of bonds was a direct consequence of the amino acid substitution or involved other parts of the interface. For Q600Y and Q600V, the increased number reflected the amino acid substitution: P3-Y had almost twice as many bonds as P3-Q. This was also true for P3-V, but to a lesser extent. For Q600F, the situation was more complex, as we observed fewer bonds to P3-F compared to P3-Y, with a higher number of bonds spread over the epitope, reflecting modest side-chain movement. This was an indirect consequence of the P3-F mutation since all other parameters were the same (resolution, space groups, crystallization conditions).

The K^b/Q600F and K^b/Q600Y structures were very similar with an r.m.s.d. of 0.36 Å (Figure 7E), with the large aromatic residues at P3 perfectly accommodated in the D pocket of the K^b binding cleft (Figure 8). In the K^b/S598 complex, P3-Gln occupies a similar position (Fig 8A); however, the larger side chains of tyrosine (Figure 8B) and phenylalanine at P3 (Figure 8C) contacted Arg155, an interaction that was not observed for the native S598 epitope or the Q600V epitope (Figure 8). Notably, while the overall structures were similar, the substitution of the P3 residue by an aromatic group changed the immediate environment of Arg155, typically a key MHC position for T cell recognition (44–46) (Figures 8B and C).

The overall structures of the K^b molecule complexed with the native S598 or Q600V were very similar (r.m.s.d of 0.33 Å on the Cα atoms). However we observed local changes in the MHC structure that likely contributed to the observed immunological differences (Figure 7F). Namely, the shorter side chain of the valine created space around the P3 residue,

allowing the side chain of Leu156 of the K^b heavy chain to reorient to reach the smaller P3 residue (Figure 8E). The conformation of Leu156 in the K^b/Q600V complex would cause steric clashes with a larger side chain at P3. The shorter P3 side chain also allowed the Arg155 guanidinium head group to move closer to the peptide, changing the position of a stretch of the α2-helix compared to that observed with the native S598 epitope (146 to 157, r.m.s.d. = 0.54 Å, maximum displacement of 0.91 Å for the Gly151 Cα). Surprisingly the Q600V peptide, like Q600Y, increased the stability of the K^b/Q600V complex compared to K^b complexed with the native S598 epitope (Figure 3). This shows that the structural rearrangements observed in the K^b molecule bound to the Q600V peptide resulted in compensatory interactions to accommodate and stabilize the shorter side chain of this buried P3 Val. Altogether the pMHC structures show that the heteroclitic peptides adopt a similar conformation to the one observed for the native S598; however they display some specific features. The Q600F and Q600Y, with a larger aromatic group at position 3, changed the environment of a key MHC residue, Arg155, by directly interacting with it. In contrast, the K^b/Q600V structure shows that a smaller side chain could be accommodated, without becoming unstable in the K^b cleft, by rearrangement of a buried MHC residue.

DISCUSSION

Heteroclitic epitopes are a subset of peptide analogues known as altered-peptide ligands that were first used to enhance T cell responses to tumors (13, 47). Since tumor antigens are self-derived, anti-tumor T cells need to escape negative selection in the thymus and tend to have low affinity for the pMHC. In contrast, high-affinity pathogen-specific T cells are not eliminated by central tolerance mechanisms so that during an infection, T cells with a broad range of affinities for their cognate antigen are recruited into the response. Despite the presence of high-affinity pathogen-specific T cells in the periphery, some of these T cell responses exhibit low functional avidity. Under these circumstances, immunization with heteroclitic epitopes provides a useful approach to enhance the functional avidity of the pathogen-specific T cell response (14). T cells with increased functional avidity are associated with more efficient pathogen clearance *in vivo* (3, 8, 48) and as we showed previously, with the prevention of CTL escape; for instance, the presence of the high functional avidity Q600Y epitope was able to prevent CTL escape at epitope S510 in mice infected with rJ (14).

Our results now highlight a possible mechanism for how such heteroclitic peptides function: heteroclitic peptides enhance pMHC stability and consequent epitope dwell time on the cell surface, thereby increasing effective surface epitope density. This induces a T cell response with higher functional avidity. This suggests that increasing the antigen density presented to T cells that typically develop a low avidity T cell response reprograms the T cell response and generates higher avidity responses. This is consistent with antigenic competition during T cell expansion that can be overcome by increasing the antigen density (49).

In this study, the relationship between total pMHC being displayed and functional avidity was first demonstrated using mice infected with recombinant VacV expressing either the S protein or an S598-minigene. After infection, K^b/S598 complexes were not detected at quantifiable levels from cells infected with VacV-S despite functional recognition of

infected cells (Figures 1B and 2A), whereas high levels of K^b/S598 were present following VacV-S598-minigene infection. This increased expression of K^b/S598 complexes resulted in greatly enhanced functional avidity of the responding cells (Figures 2B and C) and a modest increase in the magnitude of the S598-specific CD8 T cell response (Figure 2A). These observations indicate that increased display of K^b/S598 provides sufficient signal to enhance the T cell response to this normally subdominant epitope and fosters the generation of high avidity T cells. Increases in magnitude of response *in vivo* as epitope density increased have been reported previously (50, 51), but our results are in marked contrast with *in vitro* studies that showed diminished functional avidity of responding T cells (3) and an *in vivo* study showing no increase in functional avidity (52) as the surface epitope density increased. The major difference between these reports and ours is that the T cell response to epitope S598 normally exhibits low functional avidity while epitopes with high functional avidity responses were examined in the published studies. Consistent with this notion, enhancement in functional avidity of the response to epitope S510 was not observed when VacV-S510-infected mice were compared to those infected with VacV-S (Figures 2E–G). This occurred even though analogously to K^b/S598, expression of the D^b/S510 complex was detectable by mass spectrometry in VacV-S510-infected cells but not when expressed from VacV-S (Figures 1B and C).

In order to determine if heteroclitic epitopes have the same physiological effect as increasing the pMHC abundance of the native epitope, we examined the capacity of two new and one established S598 analogue to elicit high functional avidity T cell responses that cross-reacted on the wild type epitope (Figures 4 and 5). Viruses expressing each of the S598 analogues all elicited higher avidity T cell responses compared to the wild type infection, with Q600V in particular generating T cells with almost two logs greater functional avidity when stimulated with the native peptide (Figure 5). Moreover, the numbers of K^b/Q600Y or K^b/Q600V complexes were significantly greater than those of K^b/S598 from cells infected with VacV expressing minigenes (Figure 6A). Together, these results suggest that heteroclitic epitopes act in part by increasing the surface density of immunogenic and cross-reactive epitopes. Whether these results are valid for all or most heteroclitic epitopes and whether this is the sole or major basis of the heteroclitic effect of such epitopes will require further investigation. Thus, while we modified an anchor residue in the peptide that enhanced binding to the MHCI molecule, this modification may also have altered T cell binding (53), contributing to the heteroclitic effect that we observed.

The design of heteroclitic epitopes remains empiric, with the rules for determining optimal configuration not established. The two additional heteroclitic epitopes (Q600F and Q600V) that we identified augmented recognition of the native S598 epitope to a similar degree (Figures 4C–F). As Tyr and Phe are structurally similar, the Q600F would have been predicted to behave similarly to the Q600Y epitope; structural and thermostability analyses of K^b/Q600F support this conclusion (Figures 3C, 7 and 8). Less clear is why cells primed with the native epitope are able to respond to APCs coated with peptide Q600F when there is virtually no recognition of the Q600Y epitope (Figures 4A–D). The latter is not explained by gross differences in T cell populations responding to S598 and Q600Y, at least based on Vβ usage (14). The structural resemblance of the Q600F and Q600Y epitopes bound to the

K^b antigen-binding cleft blur cross-reactivity pattern differences between the two epitopes. The design of heteroclitic peptides is largely based on increased stability of the pMHC, which for most epitopes results in enhanced T cell activity. However the natural plasticity of the epitope has been shown to be crucial for some T cell receptors to dock appropriately onto their pMHC targets (54, 55). The new network interactions of the modified P3-Tyr residue with Arg155 and Glu152, observed only in Q600Y (Figure 7B), could explain the cross-reactivity pattern differences observed when K^b/Q600Y and K^b/Q600F or K^b/S598 are compared.

The second heteroclitic epitope Q600V encodes P3-Val, an amino acid that has a shorter side chain than the aromatic Phe or Tyr; the latter being the most frequently detected subanchor in the consensus K^b ligand binding motif (56). The structural rearrangement observed in the cleft of K^b facilitated stability of the complex, and might lead to reconsideration of whether P3-Val is actually a sub-optimal secondary anchor residue. Indeed, mass spectrometry-based sequencing of approximately 500 epitopes eluted from K^b, showed that while Tyr was dominant at P3 (34%), Val was detected in a significant fraction (9%) (unpublished observations). Q600V exhibited enhanced stability and presented a similar antigenic surface to the one observed for S598, thereby inducing a T cell response with nearly complete cross-reactivity with the native epitope (Figure 4G).

In conclusion, we have shown that increased expression of MHCI complexed with a peptide that induces a low functional avidity T cell response or priming with heteroclitic variants that stabilize pMHCI enhanced the functional avidity of the ensuing T cell response. The use of heteroclitic peptides provides a practical approach to induce high functional avidity T cell responses by increasing the cell surface expression of weakly immunogenic epitopes. Furthermore, we identified a heteroclitic epitope that elicits a T cell response with nearly complete cross-reactivity to the native epitope. The structural data show that these heteroclitic epitopes induce modest conformational changes in the local environment of the pMHCI complex, which will help guide the rational design of these altered ligands in the setting of vaccine development. Further, understanding T cell engagement with the pMHC complex will clearly also be important in designing effective, highly cross-reactive heteroclitic epitopes. Notably, while we analyzed T cell epitopes expressed by a murine coronavirus, the results may be useful for the design of vaccines directed against pathogenic human coronaviruses, such as SARS-CoV, which also requires a robust T cell response for efficient virus clearance (57, 58).

Acknowledgments

We thank Dr. David Tscharke for helpful discussions.

References

1. Croft NP, Purcell AW. Peptidomimetics: modifying peptides in the pursuit of better vaccines. Expert Rev Vaccines. 2011; 10:211–226. [PubMed: 21332270]
2. Purcell AW, McCluskey J, Rossjohn J. More than one reason to rethink the use of peptides in vaccine design. Nat Rev Drug Discov. 2007; 6:404–414. [PubMed: 17473845]

3. Alexander-Miller MA, Leggatt GR, Berzofsky JA. Selective expansion of high- or low-avidity cytotoxic T lymphocytes and efficacy for adoptive immunotherapy. Proc Natl Acad Sci USA. 1996; 93:4102–4107. [PubMed: 8633023]
4. Zeh HJ 3rd, Perry-Lalley D, Dudley ME, Rosenberg SA, Yang JC. High avidity CTLs for two self-antigens demonstrate superior in vitro and in vivo antitumor efficacy. J Immunol. 1999; 162:989–994. [PubMed: 9916724]
5. Gallimore A, Dumrese T, Hengartner H, Zinkernagel RM, Rammensee HG. Protective immunity does not correlate with the hierarchy of virus-specific cytotoxic T cell responses to naturally processed peptides. J Exp Med. 1998; 187:1647–1657. [PubMed: 9584143]
6. Sedlik C, Dadaglio G, Saron MF, Deriaud E, Rojas M, Casal SI, Leclerc C. In vivo induction of a high-avidity, high-frequency cytotoxic T-lymphocyte response is associated with antiviral protective immunity. J Virol. 2000; 74:5769–5775. [PubMed: 10846055]
7. Neveu B, Debeaupuis E, Echasserieau K, le Moullac-Vaidye B, Gassin M, Jegou L, Decalf J, Albert M, Ferry N, Gournay J, Houssaint E, Bonneville M, Saulquin X. Selection of high-avidity CD8 T cells correlates with control of hepatitis C virus infection. Hepatology. 2008; 48:713–722. [PubMed: 18712791]
8. Almeida JR, Price DA, Papagno L, Arkoub ZA, Sauce D, Bornstein E, Asher TE, Samri A, Schnuriger A, Theodorou I, Costagliola D, Rouzioux C, Agut H, Marcelin AG, Douek D, Autran B, Appay V. Superior control of HIV-1 replication by CD8+ T cells is reflected by their avidity, polyfunctionality, and clonal turnover. J Exp Med. 2007; 204:2473–2485. [PubMed: 17893201]
9. Bullock TN, Mullins DW, Colella TA, Engelhard VH. Manipulation of avidity to improve effectiveness of adoptively transferred CD8(+) T cells for melanoma immunotherapy in human MHC class I-transgenic mice. J Immunol. 2001; 167:5824–5831. [PubMed: 11698456]
10. Speiser DE, Baumgaertner P, Voelter V, Devevre E, Barbey C, Rufer N, Romero P. Unmodified self antigen triggers human CD8 T cells with stronger tumor reactivity than altered antigen. Proc Natl Acad Sci USA. 2008; 105:3849–3854. [PubMed: 18319339]
11. Zhang Y, Liu Y, Moxley KM, Golden-Mason L, Hughes MG, Liu T, Heemskerk MH, Rosen HR, Nishimura MI. Transduction of human T cells with a novel T-cell receptor confers anti-HCV reactivity. PLoS Pathog. 2010; 6:e1001018. [PubMed: 20686664]
12. Kessels HW, Wolkers MC, van den Boom MD, van der Valk MA, Schumacher TN. Immunotherapy through TCR gene transfer. Nat Immunol. 2001; 2:957–961. [PubMed: 11577349]
13. Dyall R, Bowne WB, Weber LW, LeMaoult J, Szabo P, Moroi Y, Piskun G, Lewis JJ, Houghton AN, Nikolic-Zugic J. Heteroclitic immunization induces tumor immunity. J Exp Med. 1998; 188:1553–1561. [PubMed: 9802967]
14. Butler NS, Theodossis A, Webb AI, Nastovska R, Ramarathinam SH, Dunstone MA, Rossjohn J, Purcell AW, Perlman S. Prevention of cytotoxic T cell escape using a heteroclitic subdominant viral T cell determinant. PLoS Pathog. 2008; 4:e1000186. [PubMed: 18949029]
15. Rosenberg SA, Yang JC, Schwartzentruber DJ, Hwu P, Marincola FM, Topalian SL, Restifo NP, Dudley ME, Schwarz SL, Spiess PJ, Wunderlich JR, Parkhurst MR, Kawakami Y, Seipp CA, Einhorn JH, White DE. Immunologic and therapeutic evaluation of a synthetic peptide vaccine for the treatment of patients with metastatic melanoma. Nat Med. 1998; 4:321–327. [PubMed: 9500606]
16. Borbulevych OY, Baxter TK, Yu Z, Restifo NP, Baker BM. Increased immunogenicity of an anchor-modified tumor-associated antigen is due to the enhanced stability of the peptide/MHC complex: implications for vaccine design. J Immunol. 2005; 174:4812–4820. [PubMed: 15814707]
17. Chen JL, Stewart-Jones G, Bossi G, Lissin NM, Wooldridge L, Choi EM, Held G, Dunbar PR, Esnouf RM, Sami M, Boulter JM, Rizkallah P, Renner C, Sewell A, van der Merwe PA, Jakobsen BK, Griffiths G, Jones EY, Cerundolo V. Structural and kinetic basis for heightened immunogenicity of T cell vaccines. J Exp Med. 2005; 201:1243–1255. [PubMed: 15837811]
18. Bullock TN, Mullins DW, Engelhard VH. Antigen density presented by dendritic cells in vivo differentially affects the number and avidity of primary, memory, and recall CD8(+) T cells. J Immunol. 2003; 170:1822–1829. [PubMed: 12574347]

19. Dzutsev AH I, Belyakov M, Isakov DV, Margulies DH, Berzofsky JA. Avidity of CD8 T cells sharpens immunodominance. Int Immunol. 2007; 19:497–507. [PubMed: 17376783]
20. Wherry EJ, Puorro KA, Porgador A, Eisenlohr LC. The induction of virus-specific CTL as a function of increasing epitope expression: responses rise steadily until excessively high levels of epitope are attained. J Immunol. 1999; 163:3735–3745. [PubMed: 10490969]
21. Rubio V, Stuge TB, Singh N, Betts MR, Weber JS, Roederer M, Lee PP. Ex vivo identification, isolation and analysis of tumor-cytolytic T cells. Nat Med. 2003; 9:1377–1382. [PubMed: 14528297]
22. Bergmann CC, Lane TE, Stohlman SA. Coronavirus infection of the central nervous system: host-virus stand-off. Nat Rev Microbiol. 2006; 4:121–132. [PubMed: 16415928]
23. van Boheemen S, de Graaf M, Lauber C, Bestebroer TM, Raj VS, Zaki AM, Osterhaus AD, Haagmans BL, Gorbalenya AE, Snijder EJ, Fouchier RA. Genomic characterization of a newly discovered coronavirus associated with acute respiratory distress syndrome in humans. mBio. 2012; 3:e00473. [PubMed: 23170002]
24. Castro RF, Perlman S. CD8+ T cell epitopes within the surface glycoprotein of a neurotropic coronavirus and correlation with pathogenicity. J Virol. 1995; 69:8127–8131. [PubMed: 7494335]
25. Pewe L, Heard SB, Bergmann C, Dailey MO, Perlman S. Selection of CTL escape mutants in mice infected with a neurotropic coronavirus: quantitative estimate of TCR diversity in the infected central nervous system. J Immunol. 1999; 163:6106–6113. [PubMed: 10570300]
26. Pewe L, Xue S, Perlman S. Infection with cytotoxic T-lymphocyte escape mutants results in increased mortality and growth retardation in mice infected with a neurotropic coronavirus. J Virol. 1998; 72:5912–5918. [PubMed: 9621053]
27. Williams RK, Jiang G, Holmes KV. Receptor for mouse hepatitis virus is a member of the carcinoembryonic antigen family of glycoproteins. Proc Natl Acad Sci, USA. 1991; 88:5533–5536. [PubMed: 1648219]
28. Anghelina D, Pewe L, Perlman S. Pathogenic role for virus-specific CD4 T cells in mice with coronavirus-induced acute encephalitis. Am J Pathol. 2006; 169:209–222. [PubMed: 16816374]
29. Croft NP, Smith SA, Wong YC, Tan CT, Dudek NL, Flesch IE, Lin LC, Tscharke DC, Purcell AW. Kinetics of Antigen Expression and Epitope Presentation during Virus Infection. PLoS Pathog. 2013; 9:e1003129. [PubMed: 23382674]
30. Tan CT, Croft NP, Dudek NL, Williamson NA, Purcell AW. Direct quantitation of MHC-bound peptide epitopes by selected reaction monitoring. Proteomics. 2011; 11:2336–2340. [PubMed: 21598389]
31. Zhao J, Zhao J, Perlman S. De novo recruitment of antigen-experienced and naive T cells contributes to the long-term maintenance of antiviral T cell populations in the persistently infected central nervous system. J Immunol. 2009; 183:5163–5170. [PubMed: 19786545]
32. Wu GF, Dandekar AA, Pewe L, Perlman S. CD4 and CD8 T cells have redundant but not identical roles in virus-induced demyelination. J Immunol. 2000; 165:2278–2286. [PubMed: 10925317]
33. Pham NL V, Badovinac P, Harty JT. A default pathway of memory CD8 T cell differentiation after dendritic cell immunization is deflected by encounter with inflammatory cytokines during antigen-driven proliferation. J Immunol. 2009; 183:2337–2348. [PubMed: 19635915]
34. Chen AT, Cornberg M, Gras S, Guillonneau C, Rossjohn J, Trees A, Emonet S, de la Torre JC, Welsh RM, Selin LK. Loss of anti-viral immunity by infection with a virus encoding a cross-reactive pathogenic epitope. PLoS Pathog. 2012; 8:e1002633. [PubMed: 22536152]
35. Kabsch W. Integration, scaling, space-group assignment and post-refinement. Acta Crystallogr D Biol Crystallogr. 2010; 66:133–144. [PubMed: 20124693]
36. Read RJ. Pushing the boundaries of molecular replacement with maximum likelihood. Acta Crystallogr D Biol Crystallogr. 2001; 57:1373–1382. [PubMed: 11567148]
37. The CCP4 suite: programs for protein crystallography. Acta Crystallogr D Biol Crystallogr. 1994; 50:760–763. [PubMed: 15299374]
38. Adams PD, Afonine PV, Bunkoczi G, Chen VB, Davis IW, Echols N, Headd JJ, Hung LW, Kapral GJ, Grosse-Kunstleve RW, McCoy AJ, Moriarty NW, Oeffner R, Read RJ, Richardson DC, Richardson JS, Terwilliger TC, Zwart PH. PHENIX: a comprehensive Python-based system for

macromolecular structure solution. Acta Crystallogr D Biol Crystallogr. 2010; 66:213–221. [PubMed: 20124702]

39. Bricogne, G.; BE; Brandl, M.; Flensburg, C.; Keller, P.; Paciorek, W.; Roversi, SAP.; Smart, OS.; Vonrhein, C.; Womack, TO. Buster version 2.10. Cambridge, United Kingdom: Global Phasing Ltd; 2011.
40. Emsley P, Lohkamp B, Scott WG, Cowtan K. Features and development of Coot. Acta Crystallogr D Biol Crystallogr. 2010; 66:486–501. [PubMed: 20383002]
41. Anton LC, Yewdell JW, Bennink JR. MHC class I-associated peptides produced from endogenous gene products with vastly different efficiencies. J Immunol. 1997; 158:2535–2542. [PubMed: 9058784]
42. Porgador A, Yewdell JW, Deng Y, Bennink JR, Germain RN. Localization, quantitation, and in situ detection of specific peptide-MHC class I complexes using a monoclonal antibody. Immunity. 1997; 6:715–726. [PubMed: 9208844]
43. Butler NS, Theodossis A, Webb AI, Dunstone MA, Nastovska R, Ramarathinam SH, Rossjohn J, Purcell AW, Perlman S. Structural and biological basis of CTL escape in coronavirus-infected mice. J Immunol. 2008; 180:3926–3937. [PubMed: 18322201]
44. Burrows SR, Chen Z, Archbold JK, Tynan FE, Beddoe T, Kjer-Nielsen L, Miles JJ, Khanna R, Moss DJ, Liu YC, Gras S, Kostenko L, Brennan RM, Clements CS, Brooks AG, Purcell AW, McCluskey J, Rossjohn J. Hard wiring of T cell receptor specificity for the major histocompatibility complex is underpinned by TCR adaptability. Proc Natl Acad Sci. 2010; 107:10608–10613. [PubMed: 20483993]
45. Gras S, Burrows SR, Turner SJ, Sewell AK, McCluskey J, Rossjohn J. A structural voyage toward an understanding of the MHC-I-restricted immune response: lessons learned and much to be learned. Immunol Rev. 2012; 250:61–81. [PubMed: 23046123]
46. Valkenburg SA, Gras S, Guillonneau C, Hatton LA, Bird NA, Twist KA, Halim H, Jackson DC, Purcell AW, Turner SJ, Doherty PC, Rossjohn J, Kedzierska K. Preemptive priming readily overcomes structure-based mechanisms of virus escape. Proc Natl Acad Sci USA. 2013; 110:5570–5575. [PubMed: 23493558]
47. Fikes JD, Sette A. Design of multi-epitope, analogue-based cancer vaccines. Expert Opin Biol Ther. 2003; 3:985–993. [PubMed: 12943457]
48. Speiser DE, Kyburz D, Stubi U, Hengartner H, Zinkernagel RM. Discrepancy between in vitro measurable and in vivo virus neutralizing cytotoxic T cell reactivities. Low T cell receptor specificity and avidity sufficient for in vitro proliferation or cytotoxicity to peptide-coated target cells but not for in vivo protection. J Immunol. 1992; 149:972–980. [PubMed: 1634779]
49. Dijkman R, Jebbink MF, Koekkoek SM, Deijs M, Jonsdottir HR, Molenkamp R, Ieven M, Goossens H, Thiel V, van der Hoek L. Isolation and characterization of current human coronavirus strains in primary human epithelia cultures reveals differences in target cell tropism. J Virol. 2013; 87:6081–6090. [PubMed: 23427150]
50. Wherry EJ, Puorro KA, Porgador A, Eisenlohr LC. The induction of virus-specific CTL as a function of increasing epitope expression: responses rise steadily until excessively high levels of epitope are attained. J Immunol. 1999; 163:3735–3745. [PubMed: 10490969]
51. Wherry EJ, McElhaugh MJ, Eisenlohr LC. Generation of CD8(+) T cell memory in response to low, high, and excessive levels of epitope. J Immunol. 2002; 168:4455–4461. [PubMed: 11970989]
52. Bullock TN, Colella TA, Engelhard VH. The density of peptides displayed by dendritic cells affects immune responses to human tyrosinase and gp100 in HLA-A2 transgenic mice. J Immunol. 2000; 164:2354–2361. [PubMed: 10679070]
53. Theodossis A, Guillonneau C, Welland A, Ely LK, Clements CS, Williamson NA, Webb AI, Wilce JA, Mulder RJ, Dunstone MA, Doherty PC, McCluskey J, Purcell AW, Turner SJ, Rossjohn J. Constraints within major histocompatibility complex class I restricted peptides: presentation and consequences for T-cell recognition. Proc Natl Acad Sci. 2010; 107:5534–5539. [PubMed: 20212169]
54. Archbold JK, Macdonald WA, Gras S, Ely LK, Miles JJ, Bell MJ, Brennan RM, Beddoe T, Wilce MC, Clements CS, Purcell AW, McCluskey J, Burrows SR, Rossjohn J. Natural

micropolymorphism in human leukocyte antigens provides a basis for genetic control of antigen recognition. J Exp Med. 2009; 206:209–219. [PubMed: 19139173]

55. Macdonald WA, Chen Z, Gras S, Archbold JK, Tynan FE, Clements CS, Bharadwaj M, Kjer-Nielsen L, Saunders PM, Wilce MC, Crawford F, Stadinsky B, Jackson D, Brooks AG, Purcell AW, Kappler JW, Burrows SR, Rossjohn J, McCluskey J. T cell allorecognition via molecular mimicry. Immunity. 2009; 31:897–908. [PubMed: 20064448]
56. Rammensee HG, Falk K, Rotzschke O. Peptides naturally presented by MHC class I molecules. Ann Rev Immunol. 1993; 11:213–244. [PubMed: 8476560]
57. Zhao J, Zhao J, Perlman S. T cell responses are required for protection from clinical disease and for virus clearance in severe acute respiratory syndrome coronavirus-infected mice. J Virol. 2010; 84:9318–9325. [PubMed: 20610717]
58. Zhao J, Zhao J, Van Rooijen N, Perlman S. Evasion by stealth: Inefficient immune activation underlies poor T cell response and severe disease in SARS-CoV-infected mice. PLoS Pathog. 2009; 5:e1000636. [PubMed: 19851468]

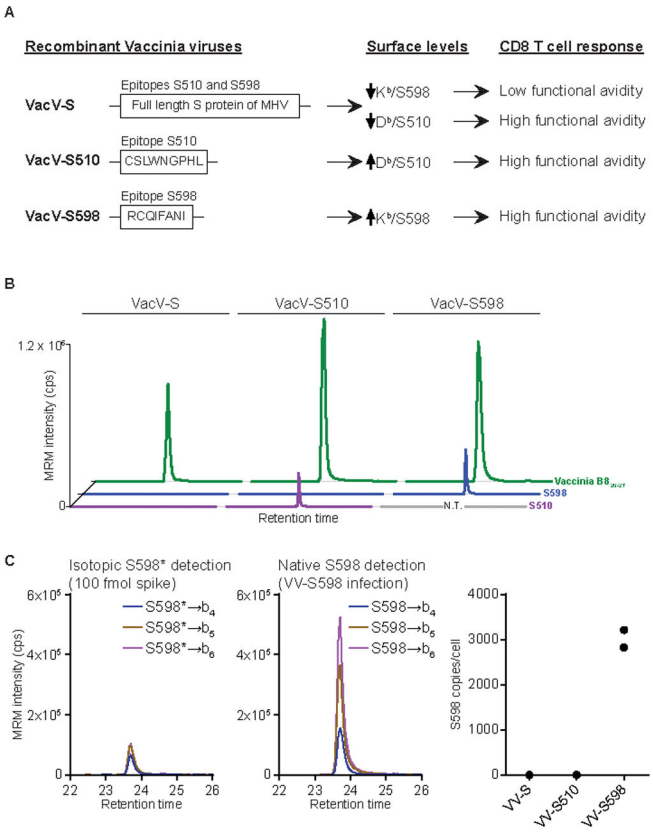

Figure 1. Detection of peptides S598, S510 and $B8_{20\text{-}27}$ complexed with H-2K/D^b

(A) Schematic of VacV constructs expressing the full length S protein of JHMV (VacV-S) or the epitopes S598 or S510 as a minigene (VacV-S598 and VacV-S510, respectively). Also shown are the relative levels of K^b/S598 or D^b/S510 exhibited by each VacV construct and the functional avidity of the responses they elicit. (B) Detection of S598, S510, and vaccinia-derived $B8_{20\text{-}27}$ eluted from H-2^b-peptide complexes at 4 hours p.i. with VacV-S, VacV-S510 or VacV-S598. Data show MRM traces (single Q1>Q3 transition shown for clarity). Data are from one of three independent experiments. C) Calculated epitope abundance of S598 from each of the VacV constructs. Isotopically labeled S598 (S598*) was introduced at the time of epitope elution to control for peptide recovery and facilitate absolute quantification. Individual Q1 Q3 transition m/z values are indicated.

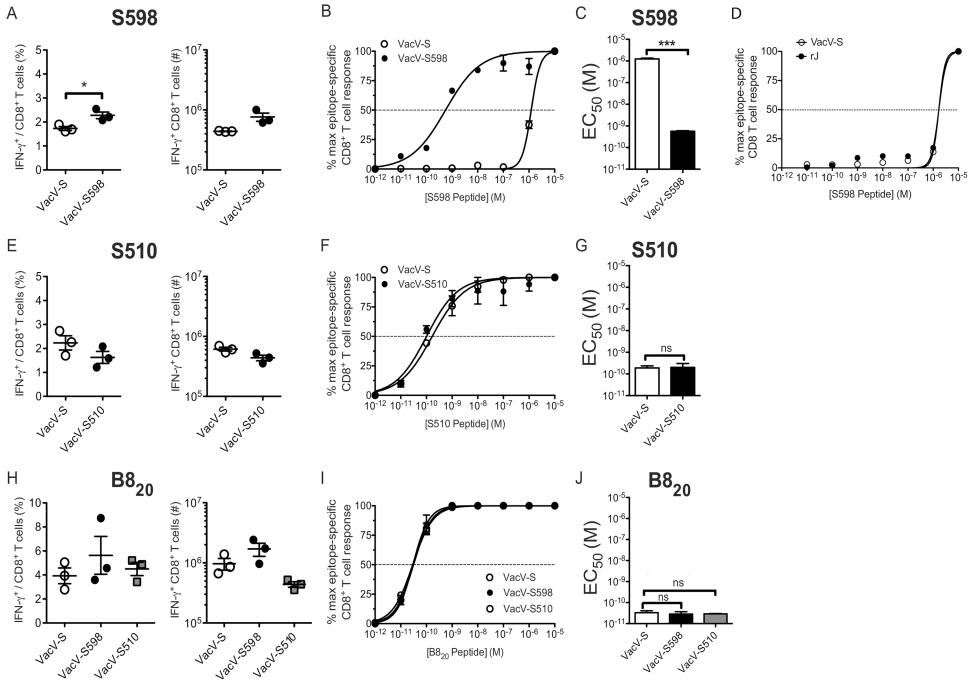

Figure 2. Increasing abundance of K^b/S598 enhances functional avidity

B6 mice were intraperitoneally infected with VacV expressing epitopes S598 or S510 as a minigene or a soluble form of the S protein of JHMV or with rJ. (A–C) Magnitude and functional avidity of S598-specific CD8 T cell response in spleens of mice infected i.p. with VacV-S or VacV-S598 at d7 p.i. (D) Functional avidity of S598-specific CD8 T cell response in spleens of mice infected i.p. with VacV-S or rJ. (E–G) Magnitude and functional avidity of S510-specific CD8 T cell response in spleens of mice infected i.p. with VacV-S or VacV-S510 at d7 p.i. (H–J) Magnitude and functional avidity of $B8_{20\text{-}27}$-specific CD8 T cell response in spleens of mice infected i.p. with VacV-S, VacV-S598, or VacV-S510 at d7 p.i. Data are representative of 3 independent experiments and presented as the mean ± SEM (n=3–4 mice/group). *p<0.05; ***p<0.001.

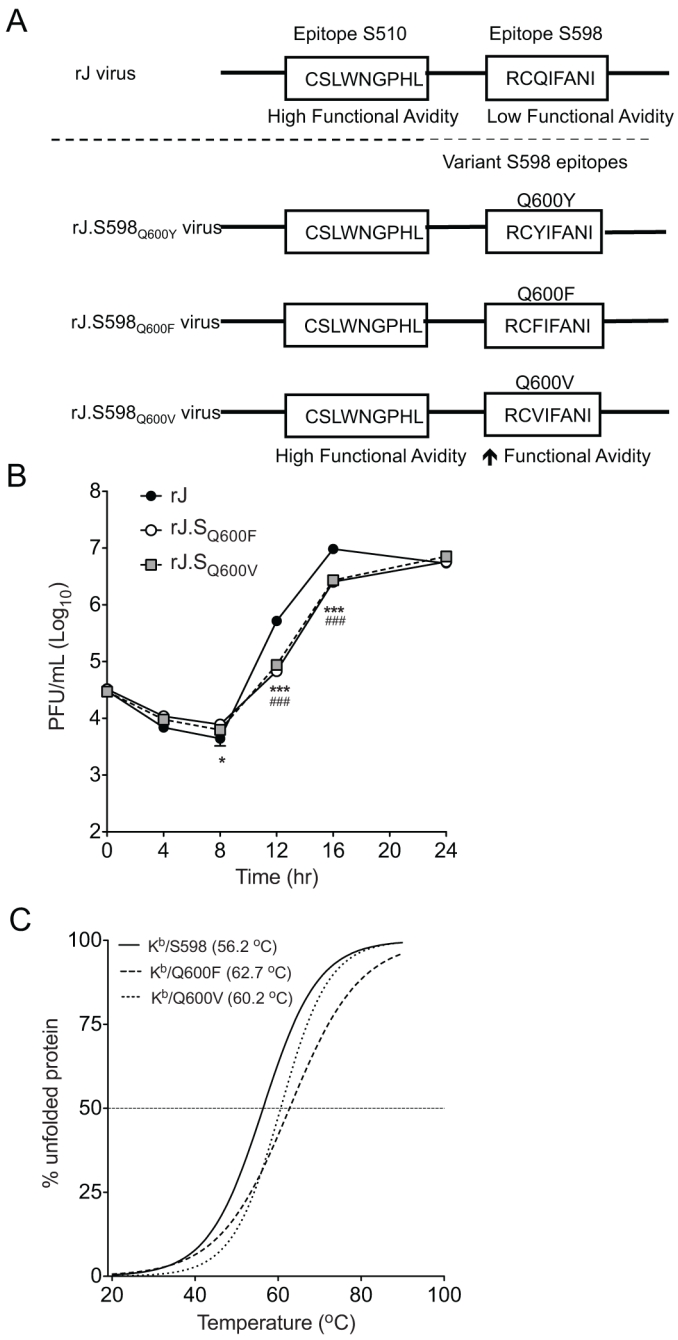

Figure 3. Development of rJ expressing S598 variants exhibiting greater K^b binding

(A) Schematic depiction of recombinant JHMV expressing native S598 (rJ), the Q600Y substitution (rJ.S_{Q600Y}), the Q600F substitution (rJ.S_{Q600F}), or the Q600V substitution (rJ.S_{Q600V}). (B) *In vitro* growth kinetics of rJ, rJ.S_{Q600F}, and rJ.S_{Q600V}. Data are representative of two independent experiments and presented as the mean ± SEM. (C) Summary of circular dichroism thermal denaturation scans of K^b/S598, K^b/Q600F and K^b/Q600V complexes used to calculate T_m (parentheses). Data are from two independent experiments.

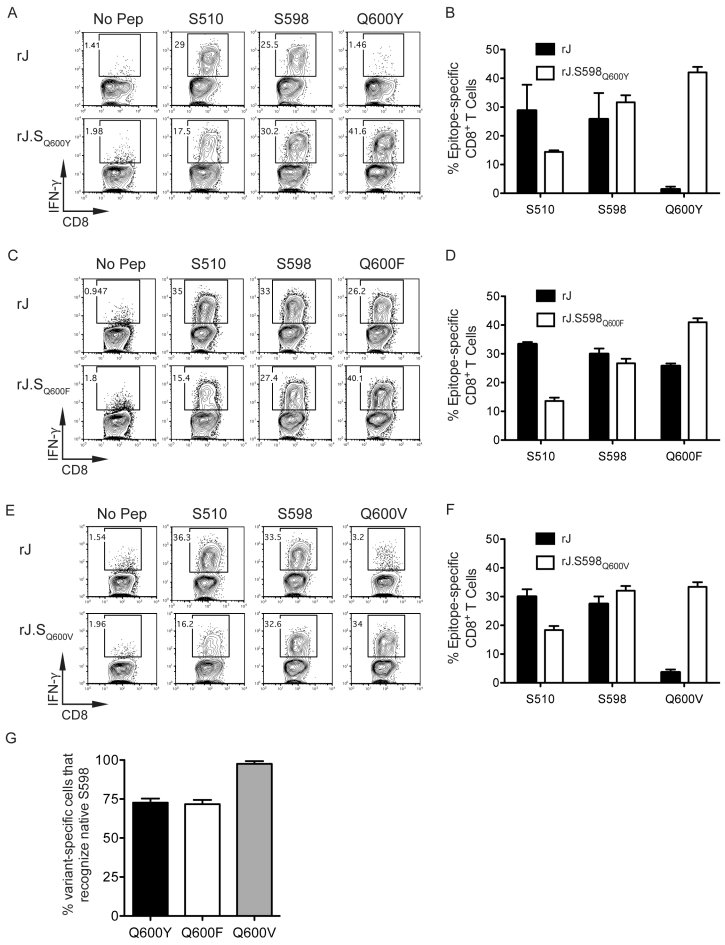

Figure 4. S598 variant epitopes induce a high proportion of S598-reactive CD8 T cells

Brain-derived leukocytes were isolated from mice infected with either rJ, rJ.S598$_{Q600Y}$, rJ.S598$_{Q600F}$, or rJ.S598$_{Q600V}$ at day 7 p.i. (A–F) Representative flow cytometry plots (A, C, E) and frequencies (B, D, F) of CD8 T cells producing IFN-γ upon stimulation with the indicated peptides are shown. (G) The percentages of variant-specific CD8 T cells that produced IFN-γ in response to stimulation with S598 peptide are shown. Data are representative of 3 independent experiments with 3–4 mice/group/experiment and are presented as the mean ± SEM.

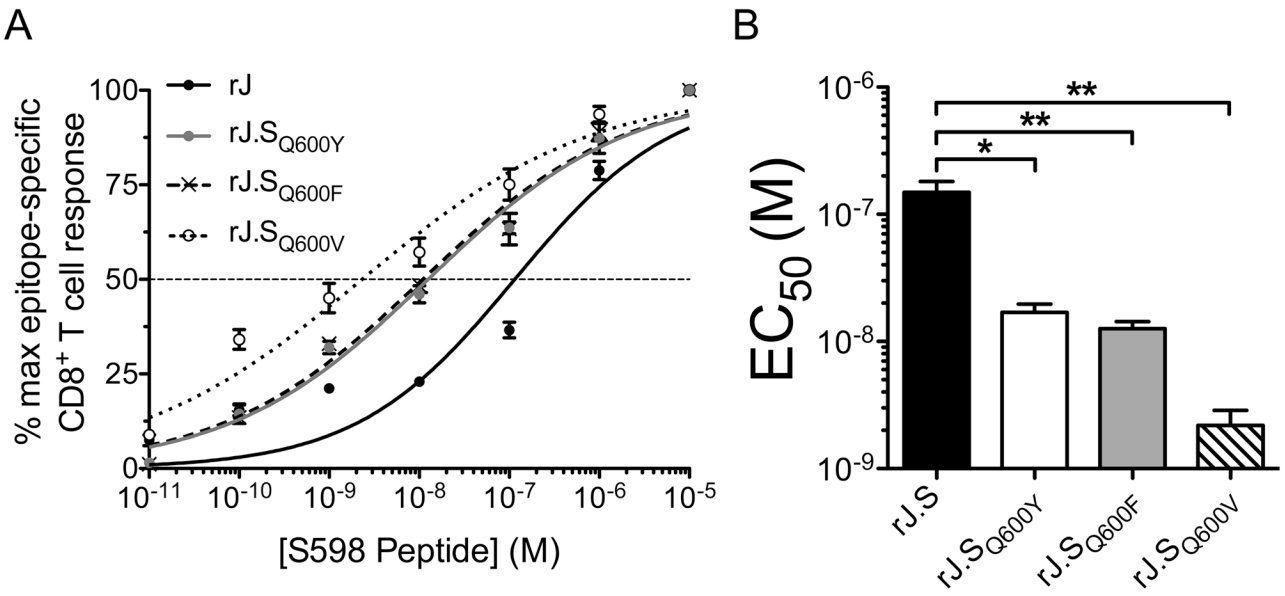

Figure 5. S598 variant epitopes, Q600Y, Q600F, and Q600V, induce higher functional avidity S598-specific CD8 T cell responses than the native epitope

Brain-derived leukocytes isolated from mice infected with either rJ, rJ.S_{Q600Y}, rJ.S_{Q600F}, or rJ.S_{Q600V} at day 7 p.i. were stimulated directly *ex vivo* with 10-fold dilutions of native S598 peptide. The percentage of CD8 T cells producing IFN-γ at each concentration was determined and normalized to the maximum frequency of S598-specific CD8 T cells detected. The data were fit to sigmoidal dose response curves (A, rJ-solid black, rJ.S_{Q600Y}-solid gray, rJ.S_{Q600F}-dashed or rJ.S_{Q600V}-dotted) and used to calculate EC_{50} values (B) for each mouse. Data are representative of three individual experiments and presented as the mean ± SEM (n=3–4 mice per group). *p<0.05; **p< 0.01.

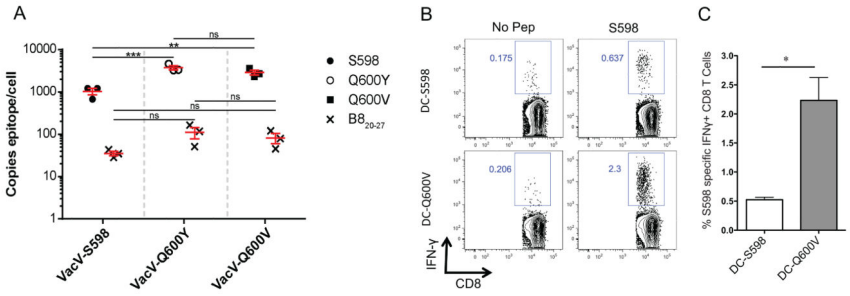

Figure 6. Abundance of native and variant S598 peptides

(A) Calculated abundance of peptides S598, Q600Y, Q600V and $B8_{20-27}$ eluted from H-$2K^b$ complexes following infection with the indicated VacV constructs. Three biological replicates are shown for each infection. Differences were analyzed using a 2 way ANOVA test. **p< 0.01; ***p<0.001. (B, C) S598-specific CD8 T cell response after immunization with DCs coated with 10 nM, 100 nM or 1 μM S598 or Q600V. Cells were stimulated with 1 μM of peptide S598 directly *ex vivo*. Representative flow cytometry plots for DCs coated with 100 nM peptide (B) and summary data (C) are shown. Summary data from one experiment with 4 individual mice are shown. Data are representative of three separate experiments.

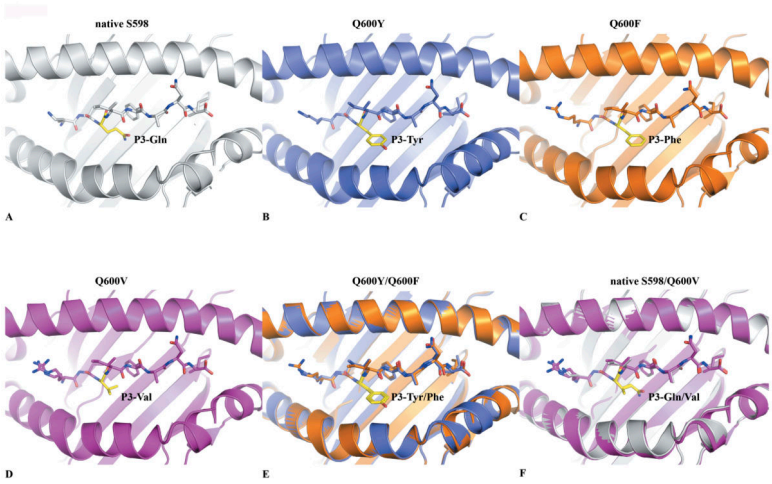

Figure 7. Structures of S598/K^b, Q600Y/K^b, Q600F/K^b and Q600V/K^b complexes

The K^b molecule is represented in cartoon with the peptide in stick; all panels are in the same orientation. The MHC is colored the same as the bound peptide: white for S598 (A), blue for Q600Y (B), orange for Q600F (C) and pink for the Q600V (D). The P3 residue is in yellow stick on all peptides. (E) Superposition of the K^b/Q600Y (blue) and K^b/Q600F (orange) complexes. (F) Superposition of the K^b/S598 (white) and Q600V/K^b (pink) complexes.

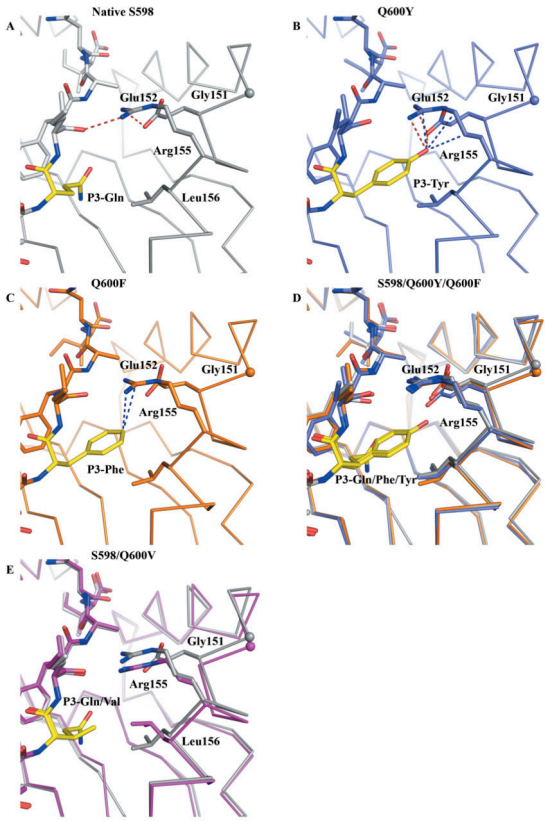

Figure 8. Detail of the antigen-binding cleft in the region surrounding position 3 of the peptide

The K^b cleft is represented as ribbon, with key residues in stick; the peptides are represented as stick with the P3 amino acid colored in yellow. The color scheme is consistent with Figure 6: K^b/Q600Y in blue (A), K^b/Q600F in orange (B), K^b/S598 in white (C), K^b/Q600Y, K^b/Q600F, K^b/S598 superimposed (D) and the K^b/Q600V in pink superimposed with the K^b/S598 on panel (E). Hydrogen bonds are represented by red dashed lines, and van der Waals interactions by blue dashed lines. The spheres represent the Cα atom of the Gly151 from the K^b molecule.

Table 1

MRM transitions used to monitor for JHMV and VACV epitopes.

Epitope	Sequence	Q1 m/z (charge)	Q3 m/z (ion)	Dwell time (ms)	Optimal CE (Collision energy)
$B8_{20-27}$ (VacV)	TSYKFESV	480.7 (+2)	609.3 (y_5)	25	28
			655.3 (SYKFE)	25	30
			756.4 (b_6)	25	22
			772.4 (y_6)	25	23
			843.4 (b_7)	25	22
			859.4 (y_7)	25	25
S598 (JHMV)	RCQIFANI	482.8 (+2)	501.3 (b_4)	40	22
			648.3 (b_5)	40	22
			719.4 (b_6)	40	22
			833.4 (b_7)	40	22
S510 (JHMV)	CSLWNGPHL	513.7 (+2)	423.2 (y_4)	40	20
			537.3 (y_5)	40	20
			723.4 (y_6)	40	20
			836.4 (y_7)	40	20

Table 2

Data Collection and Refinement Statistics

Data Collection Statistics	**H2Kb-Q600V**	**H2Kb-Q600F**
Temperature	100K	100K
Space group	**$P2_1$**	**$P2_1$**
Cell Dimensions (a,b,c) (Å)	66.47, 90.75, 89.52	66.46, 90.99, 89.61
(°)	β =111.57	β =111.65
Resolution (Å)	100 – 2.0 (2.2-2.0)	100 – 2.3 (2.5-2.3)
Total number of observations	275720 (68922)	155539 (31982)
Number of unique observations	65401 (16113)	42500 (8686)
Multiplicity	4.2 (4.2)	3.6 (3.7)
Data completeness (%)	97.7 (97.2)	96.1 (89.4)
I/σ_I	12.1 (4.3)	11.6 (3.9)
R_{merge}[a] (%)	9.7 (44.1)	7.7 (45.3)
Refinement Statistics		
Non-hydrogen atoms		
Protein	6436	6436
Water	787	401
R_{factor}[b] (%)	17.32	17.03
R_{free}[b] (%)	21.79	21.65
Rms deviations from ideality		
Bond lengths (Å)	0.010	0.010
Bond angles (°)	1.08	1.13
Ramachandran plot (%)		
Allowed region	99.2	99.0
Generously allowed region	0.8	0.8
Disallowed region	0	0.2

[a] $R_{merge} = \Sigma |I_{hkl} - < I_{hkl} >| / \Sigma I_{hkl}$.

[b] $R_{factor} = \Sigma_{hkl} ||F_o| - |F_c|| / \Sigma_{hkl} |F_o|$ for all data except ≈ 5% which were used for R_{free} calculation. Values in parentheses are for the highest resolution-shell.

Table 3

Distribution of Intermolecular Bonds

Epitope	Nb bond	VDW	HB	SB
S598	169	150	18	1
Q600Y	190	169	20	1
Q600F	194	174	19	1
Q600V	175	159	15	1